Equivalent mechanical load model methodology to simulate lightning strike impact on protected and painted composite structure

A. Bigand, Christine Espinosa, J.M. Bauchire

Equivalent mechanical load model methodology to simulate lightning strike impact on protected and painted composite structure

A. Bigand[abc*], C. Espinosa[a*], J.M. Bauchire[c]

[a] *Institut Clément Ader (ICA), Université de Toulouse, CNRS-INSA-ISAE-Mines Albi-UPS, 3 Rue Caroline Aigle, 31077 Toulouse Cedex 4, France – christine.espinosa@isae-supaero.fr*

[b] *Airbus Operations SAS,* 316 route de Bayonne, *31060 Toulouse Cedex 09, France,*

[c] *GREMI, UMR 7344, CNRS-University of Orleans, 14 rue d'Issoudun, BP 6744, 45067 Orleans Cedex 2, jean-marc.bauchire@univ-orleans.fr*

*corresponding author: audrey.a.bigand@airbus.com +33(0)5 67 19 56 87

Keywords: lightning; impact; carbon fibre reinforced plastics; numerical simulations; paint

Abstract

Lightning strike damage on aircraft composite structure is very difficult to predict. The main source of this damage is the mechanical constraint generated by the lightning in interaction with the structure made of composite, protected with a metallic mesh and painted. The purpose of this paper is to propose a numerical model able to reproduce the surface overpressure generated by the explosion of the lightning strike protection (LSP) and its confinement with the paint. Comparisons of numerical displacements with lightning experimental ones are presented in order to analyse the predictability of the model. This is a first step in order to assess the damage in the composite structure depending on the design configurations (CFRP, LSP and Paint) when combined with a damage model.

1. Introduction and context

In the last 40 years, the use of composites has significantly increased in the aircraft industry, as carbon fibre reinforced composites present a higher strength and stiffness to mass ratio compared to metallic structures. Despite their excellent mechanical properties, composites are poor conductors, making them more susceptible to serious damage due to a lightning strike such as severe delamination, burning and possibly puncture [1]. In order to protect the composite structures, a lightning strike protection layer, usually a metallic mesh, is applied on the external surface.

It is extremely difficult to predict the damage incurred by the composite structure since different types of damage occur: fibre tufting and resin decomposition on one hand, and delamination and matrix cracking on the other hand. This is indeed a highly dynamic and multi-physics phenomenon. There is no fully validated theory on all the physics phenomena involved by the arc and its interaction with the structure or the associated chronology. Still, a proposal of the different constraints involved has been developed [2] and illustrated in Figure 1. On one side, there are thermal forces with the thermal flux at the arc root, the thermal radiation from the arc channel and the joule heating from the current flow. On the other side, there are mechanical forces with Laplace forces and shock wave from the arc generation.

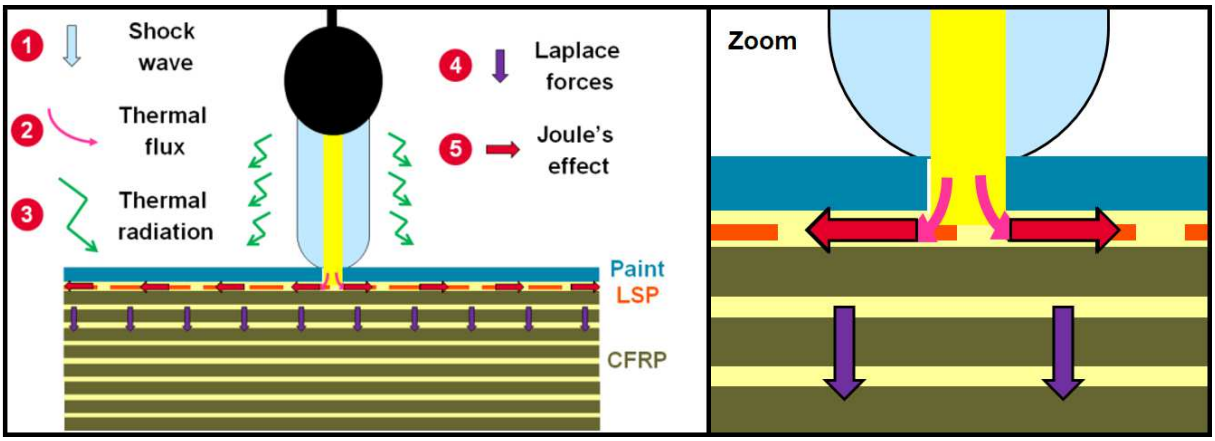

Figure 1 Lightning constraints generation in composite structures

Work performed in the past to simulate damage induced by a lightning strike, which can be found in the literature, was first based on a simple electro-thermal approach in which the current flow in the composite generates heat that will create damage [3–7]. These models were subsequently refined by considering the degradation of the resin by pyrolysis [3,6–12]. In many cases, the arc was modelled as an equivalent current source with a fixed injection area. It has been demonstrated, however, that the arc root interacts with the structure and that its injection is variable in time and space [13–15]. Finally, this approach showed its limitations since it proved unable to predict the underlying delamination coming from a mechanical constraint. In order to assess delamination, which is the most detrimental effect for the sustainability of the structure, a model of the mechanical sources generated by the arc, i.e. the shock wave and the magnetic pressure, was introduced [16–23]. However, the theory is not fully validated yet and the magnitude and distribution of these forces are highly dependent on the arc root interaction. This sensitivity makes it very difficult to weight these two contributors correctly. Even if a more accurate model could be developed, this would not suffice to predict the damage as the values of these forces that were determined were not high enough to generate significant stress in the composite [21,23].

This led some researchers to investigate the explosion effect of the composite but also the role of the metallic protection on the surface of the structure as the sudden and high lightning current flowing in the conductor leads to a rapid increase in temperature up to an explosion [16,24,25]. Finally, it is not enough to consider the different forces that can be generated by a lightning strike; it is also necessary to take into account the total system that will interact with these forces. Of course, the composite structure where damage prediction is essential is part of it. But in addition, the lightning strike protection and the paint must be introduced in the model [26]. Indeed, lightning tests on protected composite structure with different paint thickness highlighted its significant influence on the damage generation in composite structure. In Figure 2 below, the visual damage and the delamination, measured by Non Destructive Test (NDT), are compared with this increasing parameter:

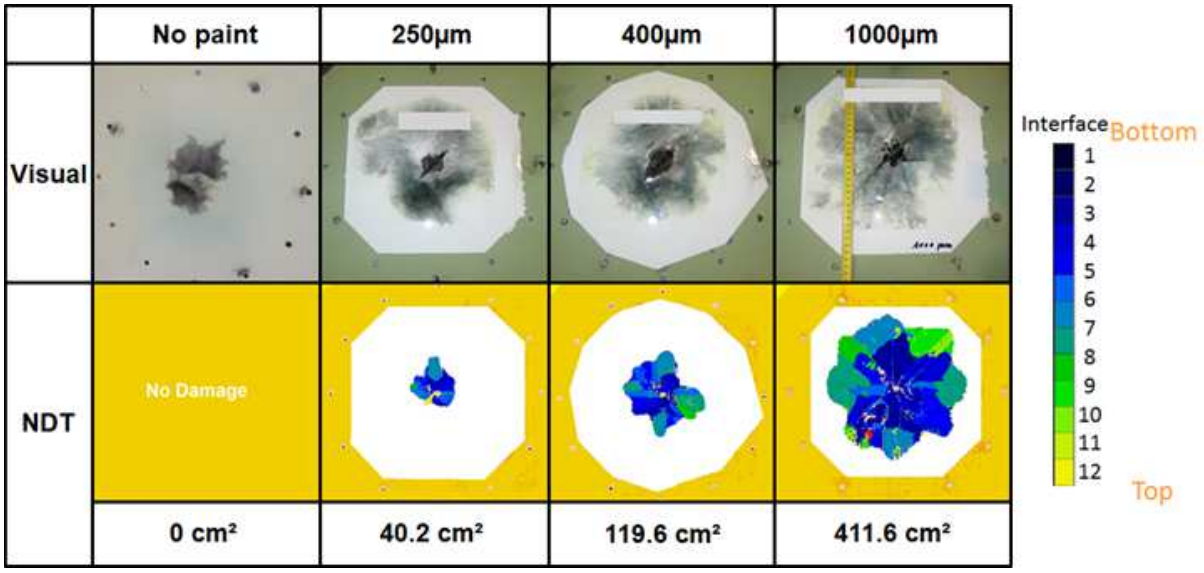

Figure 2 Lightning damage evolution in CFRP panel (13 plies) protected with ECF195 with different paint thickness

This influence is mainly due to the confinement effect of the lightning strike protection (LSP) explosion by the paint that will enhance the overpressure.

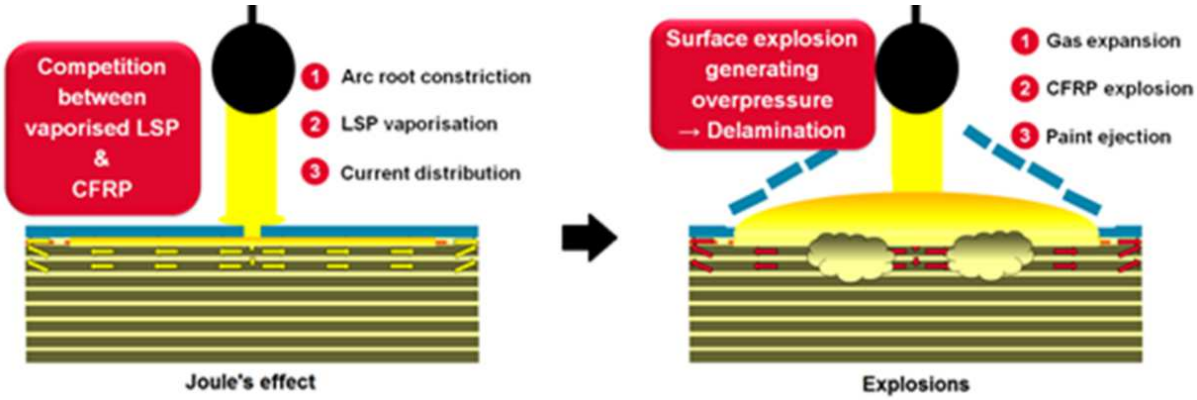

Figure 3 Lightning surface explosion

In this paper, we will present a methodology for the construction of the equivalent mechanical load due to lightning strike on a complete structure, considering the CFRP, the LSP and the paint.

2. Basis of the work

2.1. Lightning experimental results

In order to study the different parameters that play a role in the generation of lightning damage, specific lightning tests were performed during the EDIFISS project. All the samples were flat square panels of 450mm lateral dimension, mechanically and electrically perfectly bonded to a circular metallic frame through 12 fasteners distributed along its 370mm diameter. A lightning strike of 100kA following waveform D [27] is performed in the centre of the panel on the front face (side where the LSP is applied). The rear face displacement is measured thanks to the image correlation technique used by DGA-TA [28]. Two high speed cameras Photron SA5 are installed at specific angles behind the panel which has been painted with a black and white pattern calibrated through a focus frame. Pictures are taken at a rate of 262,500 frames per second (fps) with a resolution of 128x128 pixels, covering a central area of the sample of 80x80 mm2. Figure 4 illustrates the test setup:

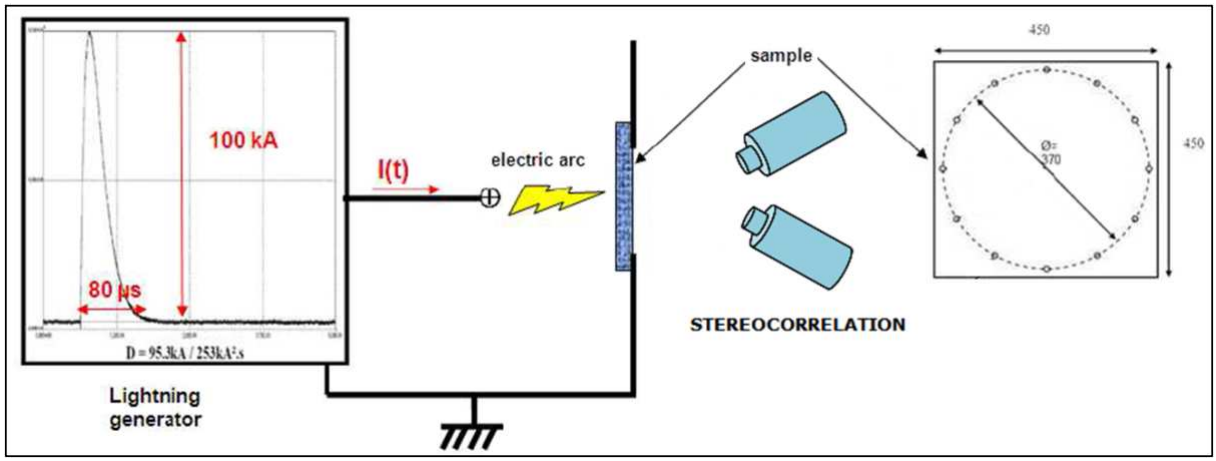

Figure 4 Lightning test setup

In a first step, the surface explosion due to Joule heating in LSP layer was studied independently from the CFRP internal damage thanks to specific tests based on the GFRP substrate. Indeed, due to its high resistivity, the lightning current will not be diverted into the glass fibre composite panel and will only flow in the metallic LSP. Therefore, the displacement of the panel is due only to the explosion occurring at the surface. Another interest of this configuration is that no damage is created in the laminate, therefore an elastic model of the panel without a damage law is sufficient to simulate its mechanical behaviour.

In a second step, CFRP substrates were tested. At the surface, the confinement effect was studied through the influence of paint thickness on the damage severity. The paint thicknesses considered were 50µm, 250µm, 400µm, and 1000µm). In the core, the influence of the global panel stiffness on the final extent of damage was studied thanks to a thicker panel. The LSP was in all cases ECF195 from Dexmet®.

A summary of the user cases is listed in Table 1 below:

Rationale	Substrate	Paint thickness (µm)
Confined surface explosion baseline	GFRP 2,75mm / 11 plies	400
Free surface explosion baseline	GFRP 2,75mm / 11 plies	**0**
Baseline CFRP structure	**CFRP 1,651**mm / 13 plies	**400**
Extreme surface confinement	CFRP 1,651mm / 13 plies	**1000**
Light surface confinement	CFRP 1,651mm / 13 plies	**250**

Stiffness influence	CFRP **3,302**mm / 26 plies	400
Stacking and CFRP grade influence	CFRP 1,651mm / **9 plies**	400

Table 1 Summary of user cases

The profile of the out-of-plane displacement along an 80 mm long line along the (x=0°) direction centred on the rear face central point is reported as a function of time. From the curves, several types of information can be extracted such as the maximum displacement and its rate at the centre versus time, or the slope and base of displacement along (x=0°) versus time. The maximum of displacement is mainly reached before 100µs. The comparison between the model and the test will be performed up to this moment. The principle is illustrated in Figure 5 :

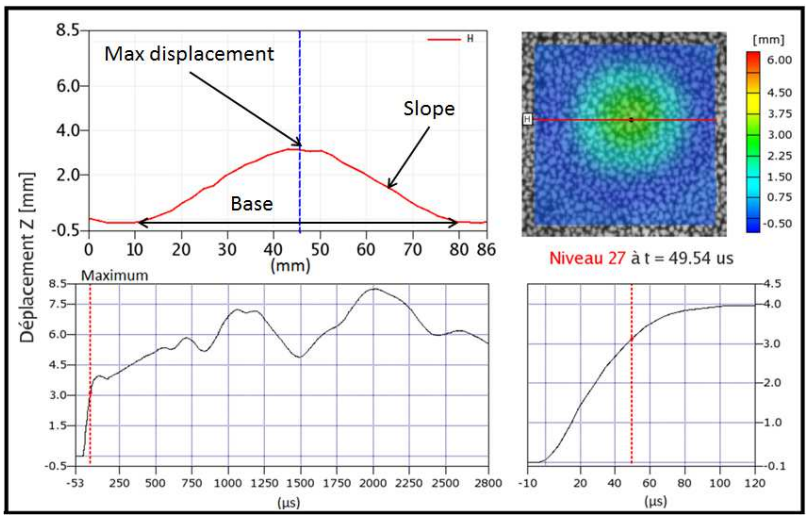

Figure 5 Rear face out of plane displacement measurement from image correlation

2.2. The surface mechanical load hypothesis

The model proposed here considers only the contributions on the surface of the composite. These contributors are the explosion of the lightning strike protection, the confinement from the paint and possibly the lightning arc shock wave. The main hypothesis taken here is that the thermal damage in the composite structure due to the lightning current flow in the fibres is negligible. This thermal source could have two different influences: the contribution

of the explosion of the composite ply in the global overpressure [29] and the modification of the composite panel mechanical properties.

2.2.1. The composite explosion

Since we cannot measure the pressure generated by a lightning strike, we measured the displacement of the back of 11 GFRP ply (2.75mm) panels protected with LSP, with or without a CFRP ply (127µm) in between, thanks to the DIC method, and painted with 400µm of typical aeronautic white paint. The added contribution of the explosion of the underlying composite ply to the total overpressure generated by the explosion of the metallic protection was limited: Rear face deflections measured without and with the underlying CFRP ply on top of the GFRP substrate were very similar. First, for the SCF configuration, the amplitudes and shapes of the measured displacement profile around the rear face centre at different instants after the test strike were quasi-identical with or without the CFRP ply. In this configuration, there was no current flowing into the LSP in opposition to ECF, therefore the overpressure was due only to explosion of the LSP. The presence of dry fibre is visible with ECF but not with SCF with 400µm of paint as illustrated in Figure 6.

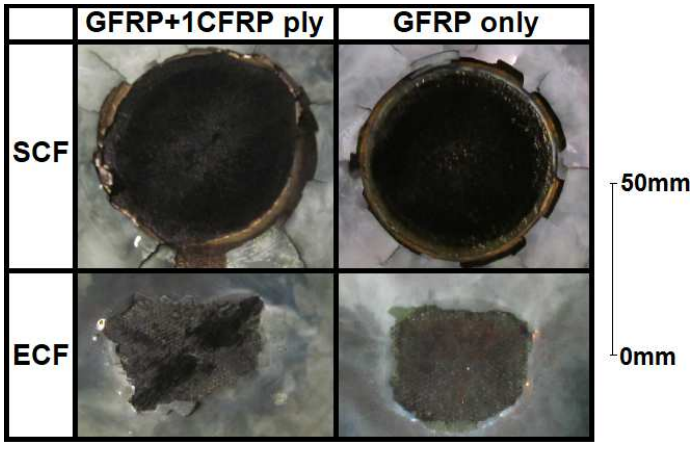

Figure 6 Visual damage observation between ECF and SCF with or without underlying CFRP ply

The deflection is not changed by the presence of the CFRP ply. Indeed, the equivalent bending modulus from the laminate theory [30] of the GFRP panel with an additional CFRP

ply at 45° is very similar to the reference GFRP panel. If we consider, in a simple approach, an equivalent shell, we can define an equivalent elastic bending modulus E_{fx} in x direction for the composite laminate:

$$E_{fx} = \frac{12}{h^3} \times \bar{E} I_{11} \quad (1)$$

With h the laminate thickness and $\bar{E} I_{11}$ the laminate equivalent elastic stiffness. From the laminate theory explicated by Gay [30], this elastic stiffness of a balanced laminate can be calculated from the bending stiffness factors C_{ij}:

$$\begin{cases} \bar{E} I_{11} = C_{11} - \dfrac{{C_{12}}^2}{C_{22}} \\ C_{ij} = \displaystyle\sum_{k=1^{st}ply}^{n^{th}ply} {\bar{E}_{ij}}^k \dfrac{({z_k}^3 - {z_{k-1}}^3)}{3} \end{cases} \quad (2)$$

The factor C_{ij} is dependent on the laminate distribution, ply orientation and property $\bar{E}_{ij}$ of each ply. The location of the ply k in the laminate depth is identified by z_k and z_{k-1}, respectively the top and bottom height positions of the ply in the laminate with the origin located in the medium plane. This stiffness coefficient $\bar{E}_{ij}$ (i,j=1..3) is a projected value of the ply coordinate system (l,t) in the global coordinate system (x,y) of the ply elastic modulus as presented in Figure 7 below:

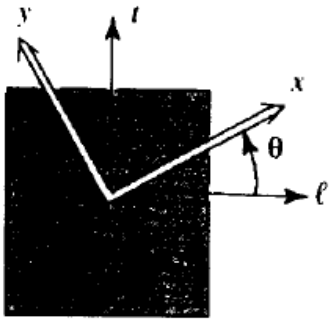

$$\begin{Bmatrix} \sigma_x \\ \sigma_y \\ \tau_{xy} \end{Bmatrix} = \begin{bmatrix} \bar{E}_{11} & \bar{E}_{12} & \bar{E}_{13} \\ \bar{E}_{21} & \bar{E}_{22} & \bar{E}_{23} \\ \bar{E}_{31} & \bar{E}_{32} & \bar{E}_{33} \end{bmatrix} \begin{Bmatrix} \varepsilon_x \\ \varepsilon_y \\ \gamma_{xy} \end{Bmatrix}$$

Figure 7 Elastic relationship projection in the global coordinate system [30]

For the assessment of the equivalent elastic bending modulus E_{fx}, we need to compute the factors ($\overline{E}_{11}$, $\overline{E}_{22}$, $\overline{E}_{12}$) for each ply orientation θ :

$$\begin{cases} \bar{E}_{11} = \mathrm{c}^4\bar{E}_l + \mathrm{s}^4\bar{E}_t + 2\mathrm{c}^2\mathrm{s}^2(\nu_{tl}\bar{E}_l + 2G_{lt}) \\ \bar{E}_{22} = \mathrm{s}^4\bar{E}_l + \mathrm{c}^4\bar{E}_t + 2\mathrm{c}^2\mathrm{s}^2(\nu_{tl}\bar{E}_l + 2G_{lt}) \\ \bar{E}_{12} = \mathrm{c}^2\mathrm{s}^2(\bar{E}_l + \bar{E}_t - 4G_{lt}) + (\mathrm{c}^4 + s^4)\nu_{tl}\bar{E}_l \end{cases} \quad (3)$$

with $\bar{E}_l = E_l/(1-\nu_{tl}\,\nu_{lt}), \bar{E}_t = E_t/(1-\nu_{tl}\,\nu_{lt})$ and c=cos θ , s=sin θ.

If we neglect that the laminate is not fully balanced with the addition of the CFRP ply on the GFRP substrate, we can calculate the bending modulus with the same approach. The GFRP plate presented a bending modulus of 24GPa and the addition of the CFRP ply change the modulus to 27GPa which is only 12% higher. The assessment of the laminate behaviour based on the flexion is limited but it provides a first framework of comparison to study the influence of such a configuration. A similar approach was used by Soulas [18] considering an equivalent bending stiffness factor, as the mean value of C_{11} and C_{22}, in order to compute an equivalent impulse.

For the ECF configuration, the influence of the presence of a CFRP layer changes the maximum amplitude of deflection slightly but also the span. The maximum deflection is lower, possibly because part of the current has been diverted to the CFRP which decreases the explosion pressure of the LSP in this area. This is illustrated in Figure 8 below on the right hand side.

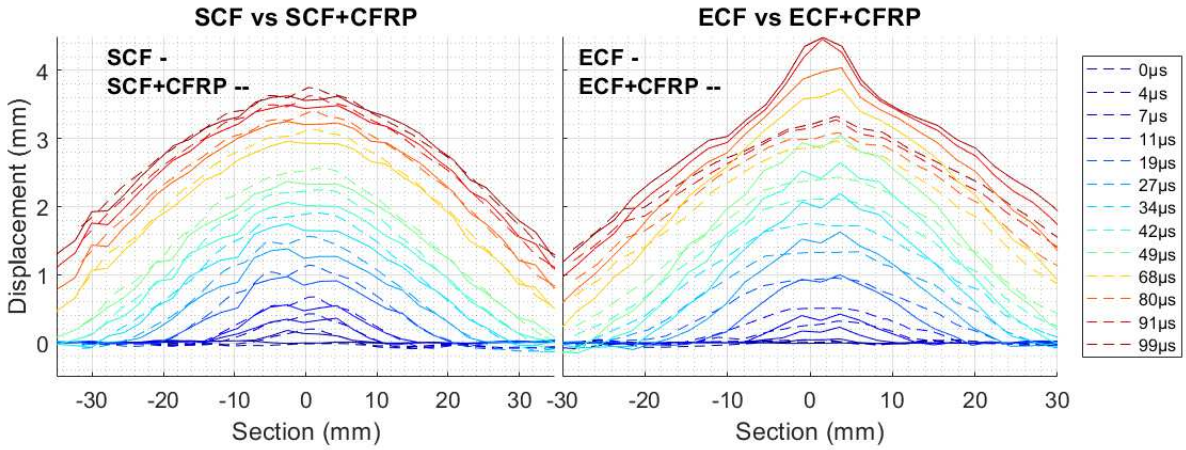

Figure 8 CFRP explosion influence on total deflection (Bump due to digital image correlation defect during test)

With these test results, we can generally, in a first stage, neglect the contribution of the CFRP explosion in the overpressure generation that will contribute to the mechanical damage. In addition, we neglect the internal damage of the CFRP due to Joule heating.

2.2.2. The thermal damage

The current flow in the composite generates Joule heating which can break the composite fibres and deteriorate the resin. This damage occurs at the same time as the mechanical load and could impinge the mechanical resistance of the panel to the impact. A thick paint applied on a composite structure constrains the arc expansion, forcing the lightning current to flow deeper in the composite than with a thinner coating. In Figure 9 below, the plies damaged by the current flow are visible thanks to a microcut done in the centre. The first ply in this section is destroyed and the second ply is highly damaged. Even with this very severe configuration where the arc root is highly constrained, the deepest ply burned is the fourth one among the thirteen plies of the panel with a total thickness of 1.65 mm.

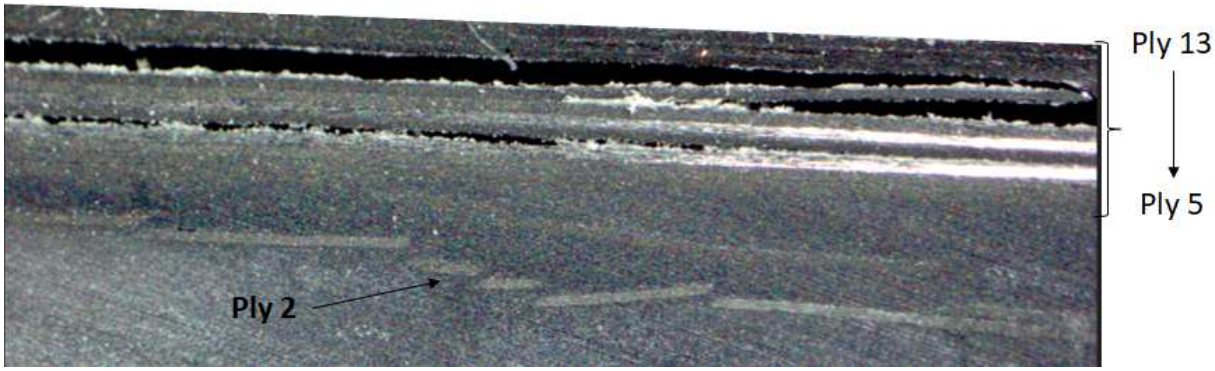

Figure 9 Internal damage study for severe configuration: CFRP (13plies) + ECF195 + 1000µm of paint

This configuration is considered severe since 1000µm of paint is not expected on an aircraft, where the usual thickness is between 250µm and 400µm. For this nominal configuration, only the first ply is burned. Due to the high electrical resistance of the composite, the current penetrates locally in the depth of the laminate but soon after flows back to the surface metallic protection. The thermal damage is therefore highly localised even for a severe configuration. Then, the thermal expansion is also supposed to be limited to these affected plies which are already damaged by Joule heating and its extension to the surrounding plies will be limited due to the slow process of heat transfer. It is therefore not expected to significantly change the mechanical behaviour of the plate.

2.3. The mechanical model

Due to the circular clamping mechanical boundary condition, only the disk in this area will be modelled and its boundary will be “encastre” in the Abaqus® input file (U1=U2=U3=UR1=UR2=UR3=0). In Abaqus/Explicit®, a single layer of shell finite elements (S3 and S4R) with elastic material properties, as defined in Table 6 5, and a user defined load (VDLOAD) on the top surface were implemented. The model proposed here considers only the contributions on the surface of the composite. These contributors are the explosion of

the lightning strike protection, the confinement from the paint and possibly the lightning arc shock wave.

	Density	E_{11}	E_{22}	G_{12}	G_{13}	G_{23}	ν_{12}	Ply thickness	Ply number	Stacking
GFRP	*1.88*	*24*	*24*	*4.8*	*4.8*	*4.5*	*0.28*	*0.25*	*11*	0° for all plies
CFRP	*1.58*	*165*	*8.5*	*4.2*	*4.2*	*3.36*	*0.35*	*0.127*	*13*	45/-45/90/45/-45/0/90/0/-45/45/90/-45/45
Unit	g/cm^3	GPa	GPa	GPa	GPa	GPa	N/A	mm	N/A	N/A

Table 2 GFRP material properties

A composite layup is defined in the shell property to simulate all the plies in the unique shell layer. Due to the quick spatio-temporal expansion of the pressure applied with the VDLOAD, the mesh is refined to 0.5mm and ordered in a square of 150mm on the centre of the disk. The mesh details are given below:

No. of elements	Element type	No. of nodes	DOF
64,090	S4R	155,026	930,156
181,468	S3		

Table 3 GFRP shell mesh details

3. Lightning equivalent load methodology

Lightning strike on a composite structure generates high overpressure due to the explosion of the lightning strike protection on its surface, enhanced by the confinement due to the presence of paint. The profile of this overpressure is not constant in time and space but variable and dependant on the lightning protection and the paint. This paragraph presents the methodology to build the surface overpressure profile equivalent to a lightning strike. Because the pressure load on the top face of the composite surface is not constant in time and space, we need to use a user subroutine that will allow us to define the magnitude of the load in Abaqus/Explicit® with a space-time function. As explained earlier, one of the main contributors is the overpressure generated by the rapid vaporization of the metallic lightning strike protection that covers the composite aircraft surface and aims at diverting lightning current. Our focus is on ECF195 which is mainly used for lightning protection. Based

231 on the development detailed in [13], the lightning strike protection is approximated in this
232 part by a web of wires of Ø125µm for this configuration. Each wire is considered as a source
233 of overpressure dependent on current density, which will generate Joule heating, which is
234 assessed as follows:

$$J_n = {}^{I_n}/_{S} \quad (4)$$

235

236 with I_n, the total injected current (100kA for waveform D) divided by the number of wires in
237 intersection with the vaporization profile and S, the section of the wire. The vaporisation
238 profile was obtained thanks to high speed camera measurements through transparent GFRP
239 panels [13]. The boundary of this profile is recorded every micro second and is
240 superimposed on the ECF pattern in order to count the number of intersections as shown in
241 Figure 10 below:

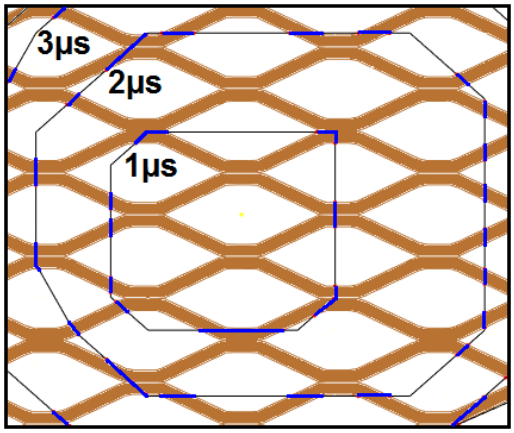

242

243 **Figure 10 Vaporisation profile intersection with ECF**

244 Since the measurement of the vaporisation profile is noisy due to the filter dependency on
245 light intensity which varies during the test, a smooth profile was developed thanks to Matlab
246 fit function in order to determine the parameter α of equation 5. For this purpose, the
247 vaporisation profile was converted into the polar coordinate system and a radius function was
248 defined per angle degree as follows:

$$R(\theta, t) = R_{max}(\theta)\left(1 - e^{-\alpha(\theta)\times t}\right) \quad (5)$$

with θ the angle, from 1 to 360°, t the time of the vaporisation profile expansion, R_{max} the maximum radius reached at θ angle direction and α a fitting parameter dependent on the angle. The function, illustrated in **Figure 11**, is therefore continuous with time and starts at zero:

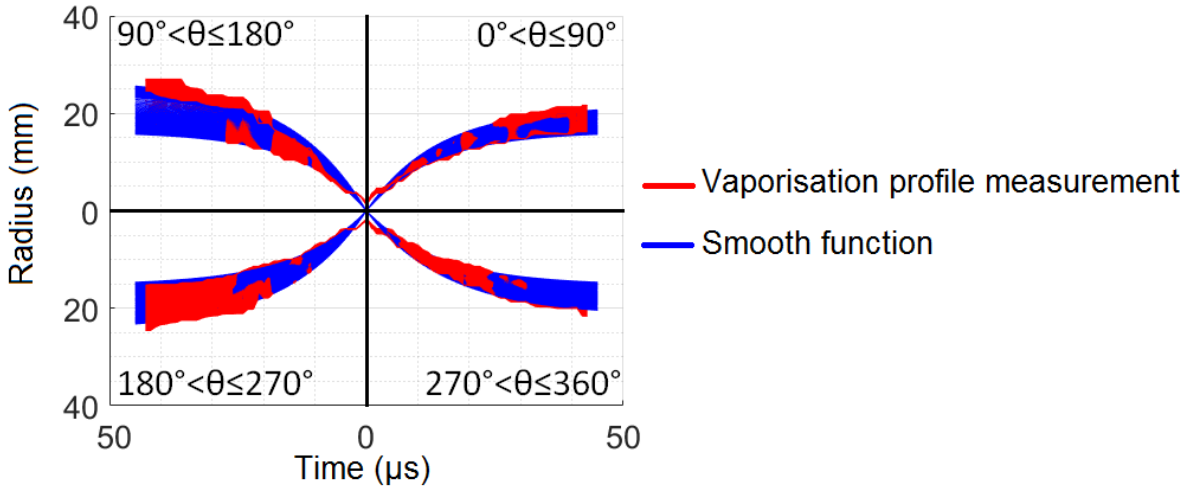

Figure 11 Radius fitting function - Angle view

The main advantage of such a definition is that it is independent from the picture sampling per µs and that it removes the variability due to measurement error, giving an increasing profile with time. This linearization of the spatial distribution of the vaporisation profile is illustrated in **Figure 12** where the profile is projected on the time axis:

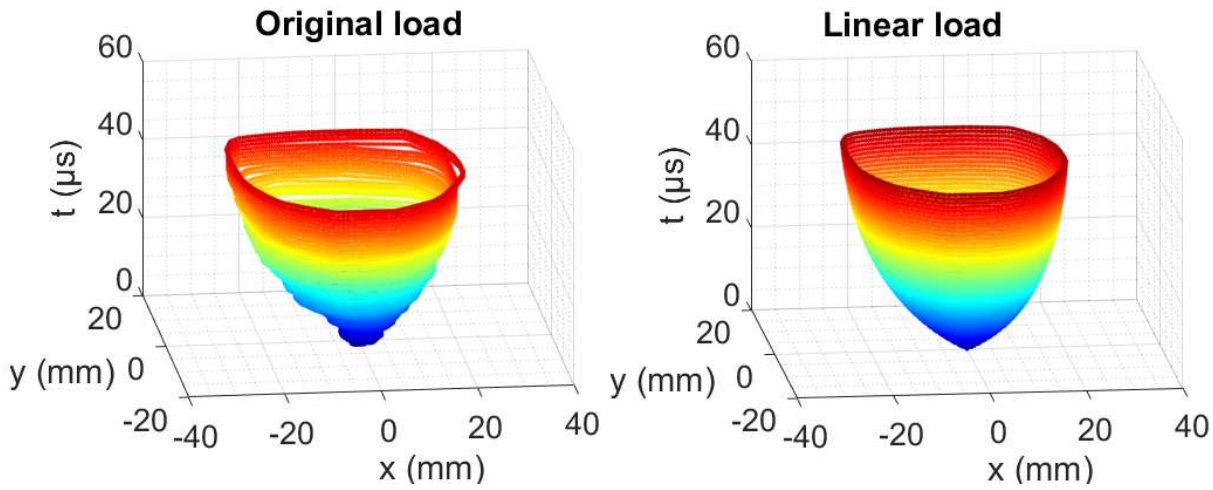

Figure 12 Vaporisation profile linearization

Based on this linearization of the spatial vaporisation, we can now assess the number of intersections per wire of ECF at each time step, as illustrated in **Figure 13** With this number, a current amplitude per wire can be defined by considering a homogenous distribution of the current along the vaporisation boundary in each wire in intersection at a given time.

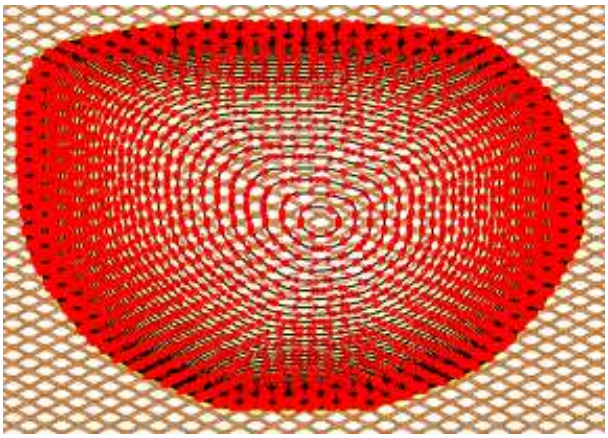

Figure 13 Intersection detection with linear vaporisation profile (ECF195+400µm of paint)

We can relate the pressure peak amplitude ΔP^+ of the wire explosion to the current amplitude I_{max} flowing in it based on experimental tests **[13]**:

$$P_{exp}(I_{max}) = a_1 {I_{max}}^{a_2} + a_3 \quad (6)$$

In this configuration, a_1=80.3 (MPa.A^{-b}), a_2=0.64 and a_3=-62.88MPa. Those parameters were determined with a function fit. Then, based on the vaporisation profile defined in the section,

we have a relationship between the explosion time and the current amplitude in the wire I_n. Therefore, we can relate the pressure peak directly to the explosion time along the vaporisation profile in order to simplify the VDLOAD as presented in **Figure 14**.

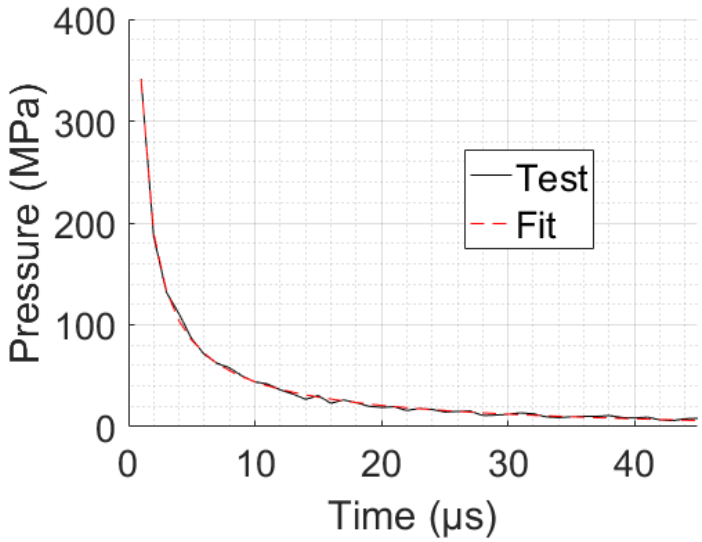

Figure 14 Shock wave peak pressure dependency on the explosion time

Knowing the vaporisation profile spatial distribution at each time step, we can associate the peak pressure amplitude with a polynomial function dependent on the explosion time thanks to Matlab fit function:

$$P_{exp}(t_{exp}) = p_1 {t_{exp}}^{p_2} + p_3 \quad (7)$$

with t_{exp} the explosion time of the wire along the vaporisation profile in µs, P_{exp} the associated peak pressure in MPa. p1=350.64812 (MPa.µs^{-1}), p2=-0.81381945 and p3=-9.6754547 (MPa) for this configuration of the ECF195 vaporisation profile confined by 400µm of paint. This process will be performed for each configuration of LSP and paint thickness since it will change the vaporisation profile, the explosion time and the peak pressure amplitude with the current density.

This function (7) will be useful for the VDLOAD, to prescribe the pressure load in each finite element at each instant. Note that, nevertheless, it uses the initial position of the grid to

291 determine the maximum pressure. Consequently, to apply the corresponding pressure, it is
292 necessary to locate the initial position of the application point.
293 Indeed, in reality, during the load application, a deflection of the sample will occur, thus in the
294 numerical model the finite element mesh cells are expected to move as well from their original
295 position. Therefore, the comparison of the element location with the vaporisation profile
296 distribution will lead to "jumps" in the load condition and an unexpected variation of the
297 pressure with time. Unfortunately, in the source file of an Abaqus® VDLOAD subroutine, it is
298 not possible to identify each mesh element number individually which could have been an
299 easy way to locate its initial position and assign a pressure history. In order to solve the issue,
300 the VDLOAD was not applied on a single top surface but on several surface elements. To
301 achieve this, the mesh coordinates of the composite front surface defined in the Abaqus®
302 '.inp' file were reviewed and superimposed with the space-time vaporisation profile. Each
303 square mesh face of 0.5mmx0.5mm, that is included in the total load profile, was clearly
304 identified and an explosion time was associated. In this case, 4429 elementary surfaces were
305 defined. The '.inp' file was modified to include the elementary surfaces, called "Surf_XXXX"
306 with XXXX the element number defined, and its associated load called "Load_ XXXX". Apart
307 from the '.inp' modification, a text file was created in which an explosion time is associated to
308 the load n°XXXX. During the computation, the VDLOAD applies the load XXX on the associated
309 surface XXX with an amplitude dependent on its associated explosion time as defined in **Figure**
310 **15**:

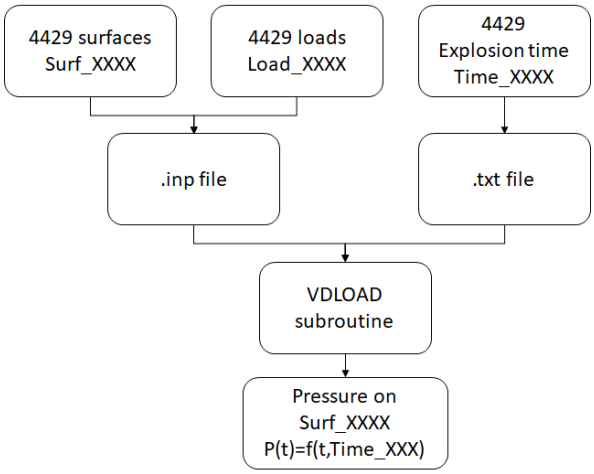

Figure 15 VDLOAD inputs

The VDLOAD subroutine calls the text file and identifies the explosion time. Therefore, each load cell is identified and its maximum pressure can be defined thanks to the equation 9 established above based on its explosion time.

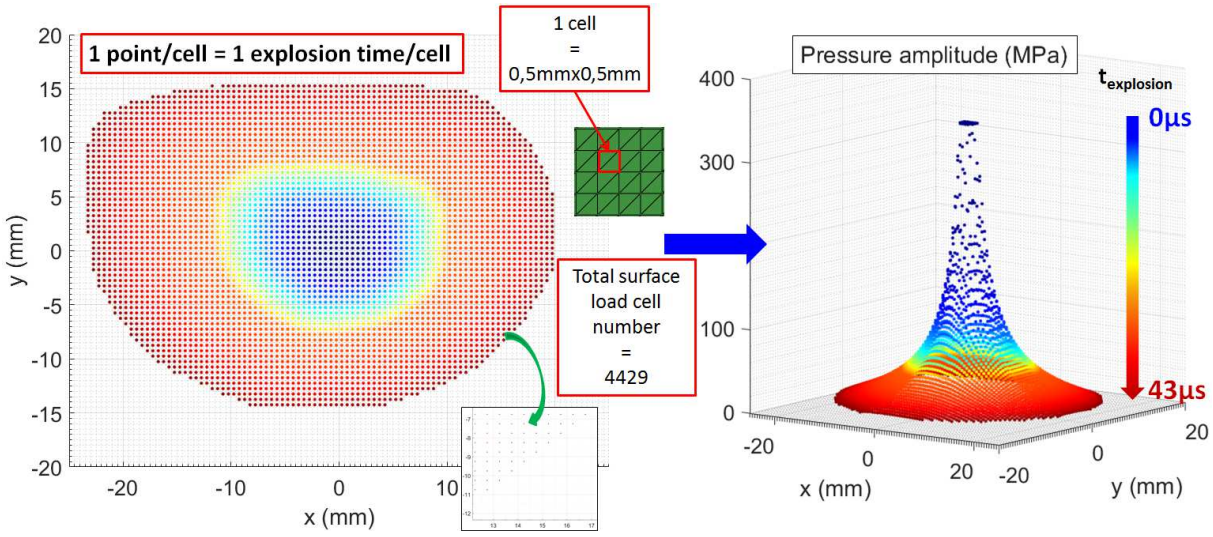

Figure 16 Vaporisation profile projection on mesh grid

As shown in **Figure 16**, the vaporisation profile defined as a function of time t and space (x,y) was projected and the explosion time is identified at the centre of each cell. One cell is one square of the mesh on the top face of the composite panel modelled. In our case, the first composite ply orientation is oriented at 45°, therefore one cell is made of 2 prismatic finite elements' top faces.

The pressure profile per cell will be defined as shown in **Figure 17**. Before the explosion time associated to the cell, no pressure is applied. Then, the pressure linearly increases up to its maximum as defined by equation **8** in Δt_{peak}=0.1µs. In theory, the time to peak for a shock wave is considered null but a small Δt is introduced to limit numerical discontinuities. After reaching its maximum, the pressure decreases. The decrease shape and duration (Δt_{decay}) should depend on the confinement. For a free explosion of the LSP, i.e. an unpainted panel, the pressure shape is considered similar to the shock wave law based on the Friedlander equation:

$$\mathrm{P(t)} = P_{exp}\mathrm{e}^{-(\mathrm{t}-\mathrm{t_{explosion}})/\Delta t_{decay\_free}} \times \left(1 - (\mathrm{t} - \mathrm{t_{explosion}})/\Delta t_{decay\_free}\right) \quad \textbf{8}$$

The decay time Δt_{decay_free} is considered dependent on the amplitude of the explosion where the decay is longer with the pressure amplitude decrease. For a confined configuration where a paint layer is present above the LSP and confines the gas of the explosion, this quick decay of the pressure cannot be considered anymore. Several shapes of pressure decay dependent on decay duration were tested and will be presented in the next section. The decay duration is defined dependent on the pressure ratio between the maximum pressure P_{max} that will be applied on the panel, corresponding to the most central area where the current density is the highest, and the cell pressure of explosion P_{exp}. Indeed, our hypothesis is that a high pressure amplitude will quickly eject the paint above and release the pressure. In the meantime, the pressure is almost fully maintained. When the pressure produced by the explosion decreases as the Joule heating in the LSP is lowered, it will delay the ejection of the paint and the pressure will be applied during a longer period.

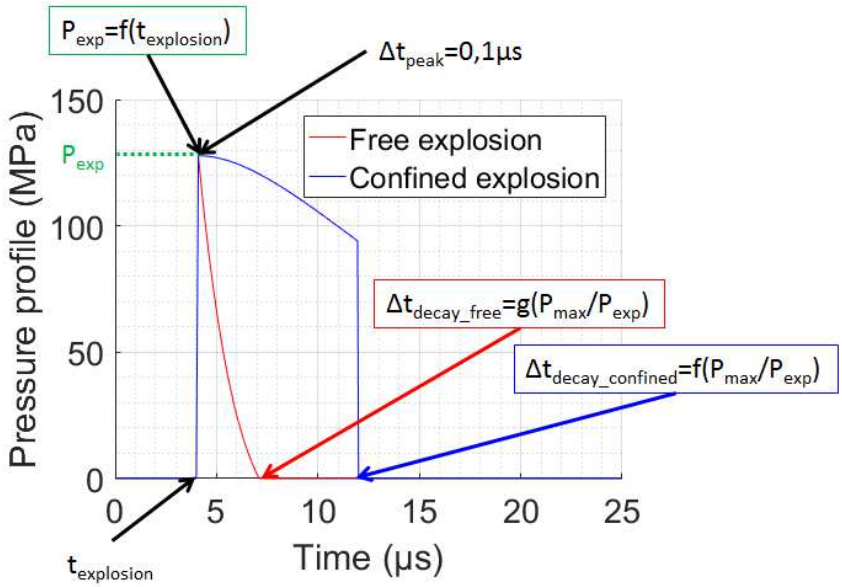

345

346 **Figure 17 Pressure profile for VDLOAD**

347

348 # 4. Results and analysis

349 ## 4.1. Surface explosion validation

350 In order to validate the contribution from the surface explosion only, a simulation for GFRP
351 panels was performed. As already mentioned, specific lightning tests have been performed
352 in laboratories where different LSP have been applied on a GFRP substrate which has the
353 main advantage of being highly resistive. Therefore, all the lightning current will flow in the
354 metallic protection, leading to its explosion. With this configuration, no delamination or
355 Joule heating occur in the laminate, thus the substrate can be simulated with a simple elastic
356 behaviour. The VDLOAD subroutine is used to apply a pressure profile dependent on time
357 and space as described earlier. The only unknown is the decrease in the pressure when the
358 metallic explosion is confined by paint or free. We have thus simulated several load
359 configurations in order to assess the influence of the decay on the panel deflection.

4.1.1. Free surface explosion

In a first step, we considered the free explosion of the LSP with different decay times Δt_{decay}. It was not possible to use the method defined in [13] to derive a space-time vaporisation profile, since the light coming from the arc column was not filtered in the absence of paint and disturbed the light capture. Therefore, we used the vaporisation profile simulated with COMSOL® [31] since it presented good correlation with the experimental melting profile. The pressure decay follows this Friedlander law defined above.

The displacement due to a free explosion of ECF195 is very limited. For the GFRP configuration, the maximum displacement after 100µs is only around 1mm compared to almost 4mm for a confined explosion with 400µm of paint as shown in Figure 18 below:

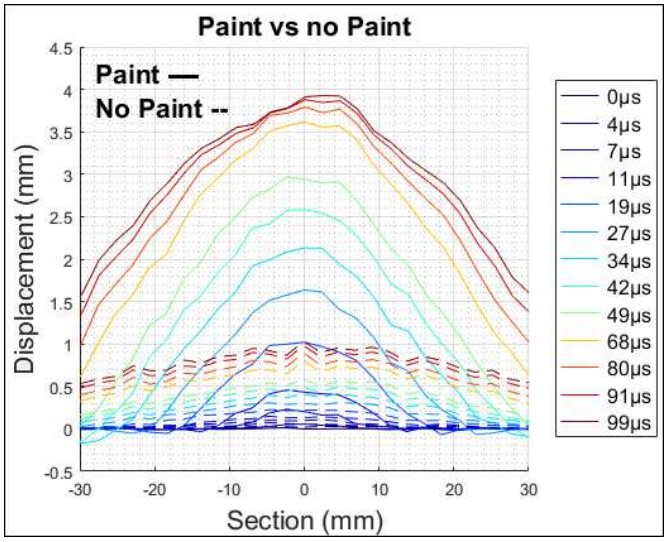

Figure 18 Displacement profile comparison: Paint vs no Paint

Considering a uniform decay time over the loaded faces no matter what the explosion pressure amplitude, or considering a decay time inversely proportional to the peak pressure resulted in displacement profiles that were never really comparable to the test result: the displacement profile was too sharp at the start of the deflection, then too slow and the displacement away from the vaporisation profile area was not negligible compared to the central area. This led us to the conclusion that a contributor was missing. Since no current

can flow in GFRP panel protected with ECF195, there is no thermal stress due to Joule heating in the panel and any thermal deformation due to heat transfer will occur on a later stage [32] as it is a slow process compared to surface explosion. This is not supposed to be the missing contributor and we surmised that it could be the acoustic shock wave from the arc column. We therefore added this pressure to the LSP explosion pressure taking into account the definition proposed by Karch [33]. This is an easy-to-use and very pragmatic approach which does not consider any Magneto-Hydro-Dynamic (MHD) effect but provides and gives the correct order of magnitude and can be implemented easily in a VDLOAD. The spatial distribution is a growing disk of a radius R depending on time:

$$\mathrm{R(t)} = 1.004 \times \left(\frac{E_0}{\rho_0}\right)^{0.25} \sqrt{t} \qquad 9$$

with ρ_0 the initial air density (kg/m^3) and E_0, the initial arc energy density (J/m). The latter parameter is a function of the maximum amplitude of the lightning current I_{max}:

$$E_0 = 0.45 \times 10^{-2} (I_{max})^{1.25} \qquad 10$$

Then, the amplitude of the shock wave can be defined as follows:

$$\mathrm{P}(\eta, \mathrm{t}) = 0.18 \times (\rho_0 E_0)^{0.25} \times \frac{\mathrm{f}(\eta)}{t} \qquad 11$$

with f(η), defined in [33], a dimensionless shape function dependent on the ratio of the radius within the pressure disk and the shock front radius: η=r/R(t). The shockwave pressure is shown in Figure 19, from 1µs to 100µs, illustrating that a pressure is maintained after the shock front passage and slowly decreases:

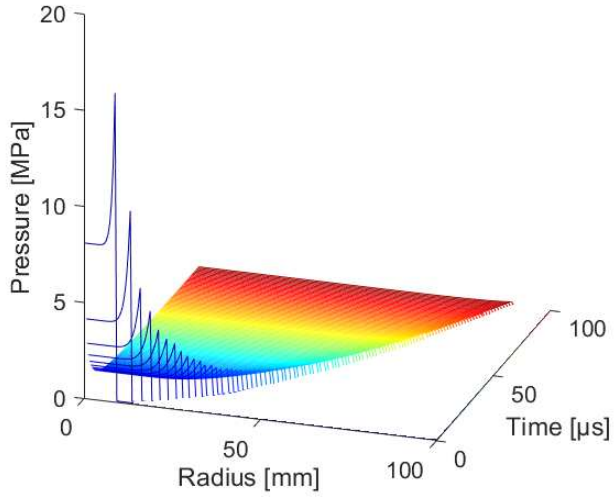

Figure 19 Shock wave pressure distribution

Looking at the contribution of the shock wave only on the panel deflection, we can conclude that its contribution is about half the maximum displacement, and so is not negligible compared to a free surface explosion, as illustrated on Figure 20:

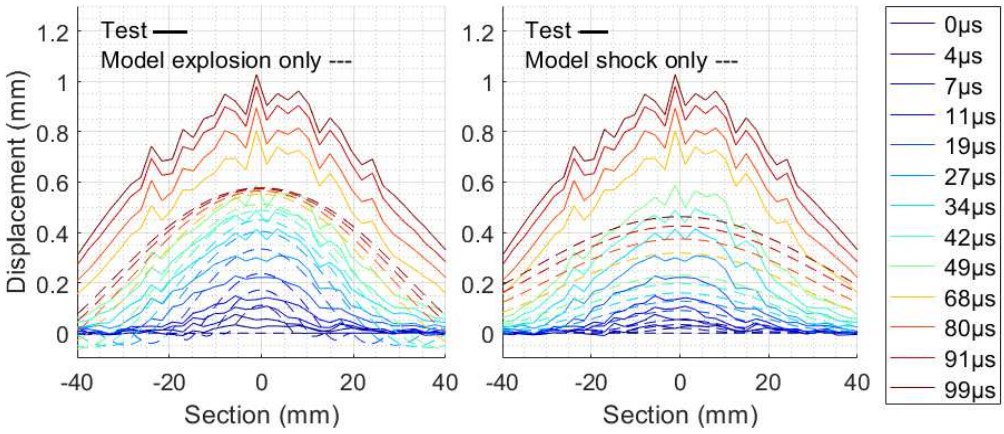

Figure 20 GFRP displacement comparison between free explosion lightning test and simulated contribution of explosion only (left) or shock only (right)

Finally, summing both contributions of the arc shock pressure coming from outside the LSP and the explosion of the LSP, the displacement of the GFRP panel, protected with ECF195, unpainted and subjected to lightning waveform D is well simulated (see Figure 21). The decay time for the explosion is inversely proportional to the peak pressure and the minimum decay time in the centre is equal to 0.85µs. A comparison of rear face deflections with the LSP surface explosion alone and with the addition of the shock wave is presented in Figure 21.

Since the explosion is quickly released, the overpressure generated on the panel is limited, hence the need to take into account the shock wave overpressure which lasts longer.

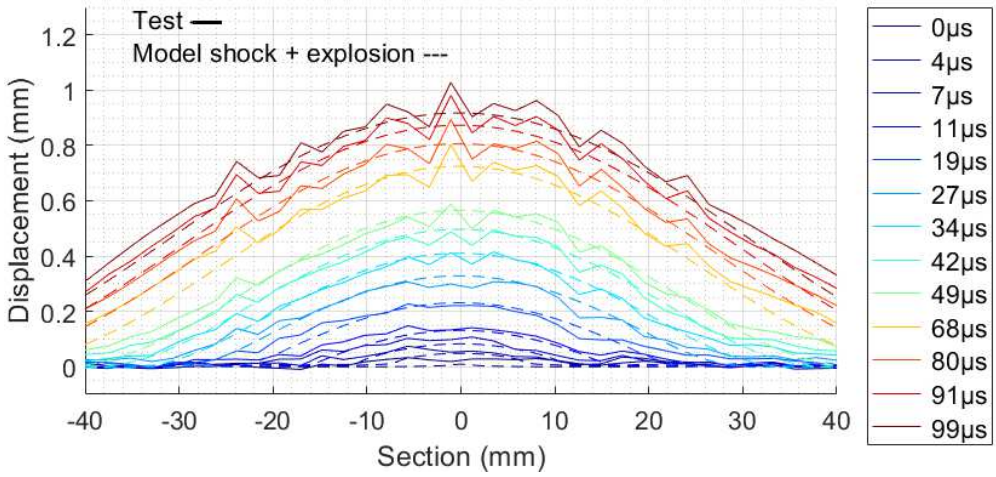

Figure 21 GFRP displacement comparison between free explosion lightning test and simulated contribution of explosion and shock wave

This first step without any confinement due to the paint highlights that the approach of the overpressure due to the explosion as a free shock wave is a fairly good hypothesis but the shock wave due to the lightning arc generation cannot be neglected. In order to support the validation of this approach, other configuration of lightning strike protection with a different profile of explosion is necessary.

4.1.2. Confined surface explosion

In a second step, we will now consider a more complex configuration: the displacement of a GFRP panel, protected with ECF195 and painted. For this case, the deflection of the panel will be enhanced since the surface explosion is confined by the presence of the paint. Adding only the same pressure as for an unpainted plate subjected to the shock is no longer valid because the paint confines the explosion pressure which is also different due to the arc constriction. The space-time distribution comes from the vaporisation profile measurement

[13]. It is therefore necessary to propose another method to estimate the pressure decay after the maximum value given by the explosion.

In order to compare the influence of different explosion profiles with the lightning test result, we chose to consider two criteria of the panel displacement. First, the maximum rear face displacement which occurs at the centre and second, the maximum of the deflection slope ε as defined in Figure 22, will be recorded. The maximum slope is computed on the horizontal and central cross section of the centre point displacement profile.

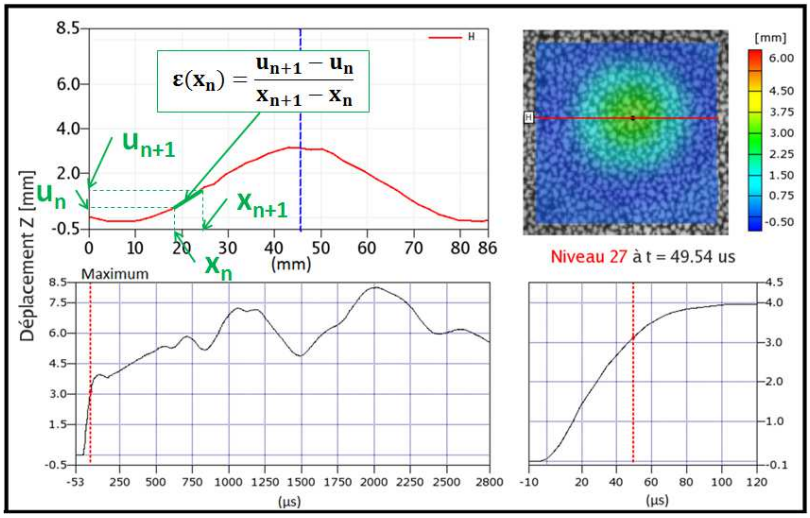

Figure 22 Maximum strain definition

Since the effect of the confinement on the explosion is not fully known, different pressure decay waveforms are considered and implemented as a surface load through a VDLOAD. The first configuration sets a constant decay time Δt_{decay} for all elementary loads, whatever the pressure amplitude. The different decay times considered were 25, 20, 15, 10 and 3.2µs. The pressure decay followed the defined law, illustrated in Figure 17:

$$P(t) = P_{exp} e^{-(t-t_{explosion})/\Delta t_{decay}} \times \left(1 + (t - t_{explosion})/\Delta t_{decay}\right) \quad 12$$

On Figure 23, it is clearly visible that a uniform decay time cannot generate the equivalent overpressure. Compared to the test, the max slope is too steep in the early stage as for the

maximum displacement. The configuration that is closest to the maximum of displacement and slope in the latest stage is the configuration with 15µs of decay. This approach cannot represent the overpressure generated on the whole surface. The paint will be ejected depending on the stress generated by the overpressure on the paint. As this overpressure decreases with the current density decrease in the ECF, the paint will take longer and longer to be ejected. The decay time will thus increase with the increase of distance from the centre [13].

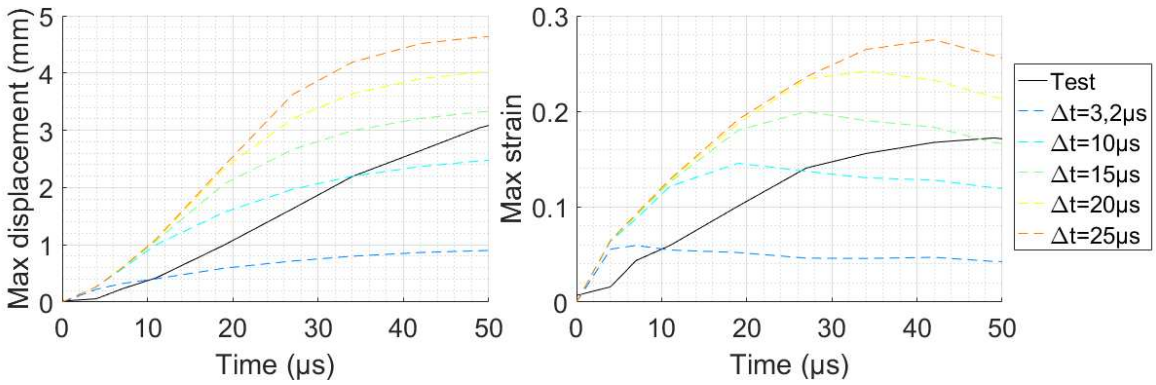

Figure 23 Overpressure sensitivity analysis with constant decay time

The second configuration considered has a decay time Δt_{decay} which increases with the inverse of the pressure decrease. Several values chosen a priori were considered: 1, 2, 3, 5 and 10µs. As shown in Figure 24, the law which provides the closest deflection behaviour is the one with the minimum decay of 3µs in the centre but again, the max slope and displacement are higher in the early stage.

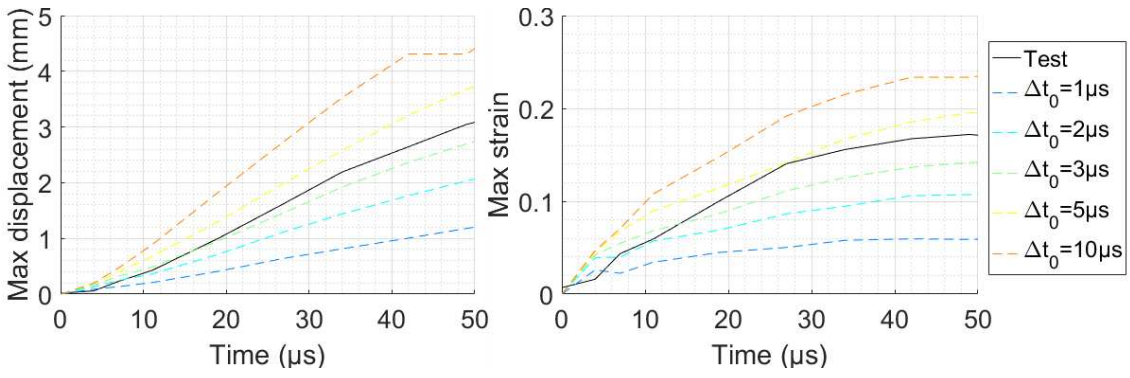

Figure 24 Sensitivity analysis of overpressure with inverse decay law – max strain

For this configuration, no shock wave is applied since its contribution cannot be applied directly on the panel, no matter what the configuration of the explosion since the ejection of the paint will disturb the overpressure applied after the shock front. It is too complex to simply add it as another contributor of the total overpressure to the LSP explosion. In our approach, we simulate a confinement of the paint with a chosen decay time and introducing the shock wave would not make a lot of sense. This approximation should not increase the error significantly since the deflection due to the lightning arc shock wave on the GFRP panel is less than a maximum of 0.5mm after 100µs compared to a total deflection of almost 4mm at the same time when there is a confinement with 400µm of paint. The final decay law chosen for this specification configuration is:

$$\begin{cases} \Delta t_{decay} = \Delta t_0 \left(\frac{P_{max}}{P_{exp}} \right)^{\alpha} \\ \Delta t_0 = 3\ \mu s\ and\ \alpha = 0.8 \end{cases} \quad (13)$$

P_{max}=max(P_{exp}) is the maximum pressure explosion reached in the centre where the current density in the copper wire is the highest. Δt_0 is the decay time in the centre and the shortest one to represent the fastest paint release due the highest explosion pressure.

The parameter α drives the decay time increase with the explosion pressure decrease as shown in Figure 25:

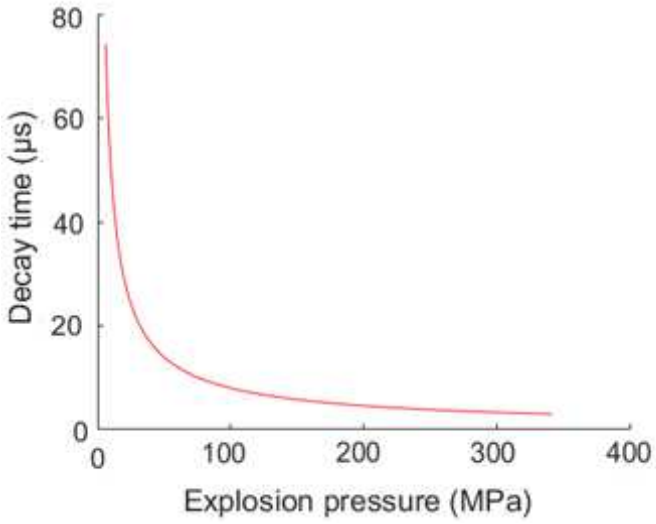

Figure 25 Decay time as a function of the explosion pressure

In addition, the pressure profile was linearized as shown previously in Figure 12. This pressure profile is the highest in the centre in one point. However, this is not related to any physical phenomenon. Therefore, the pressure load applied in the centre will be on a disk corresponding to the first measured disk in the back light measurement of the vaporisation profile. The diameter of this disk is smaller than 4mm.

The deflection measurement of the GFRP panel protected with ECF195 and confined by 400µm of paint during the lightning test performed with WFD is compared with our simulation with the VDLOAD following the decay law defined in Equation 6 36 and is presented in Figure 26:

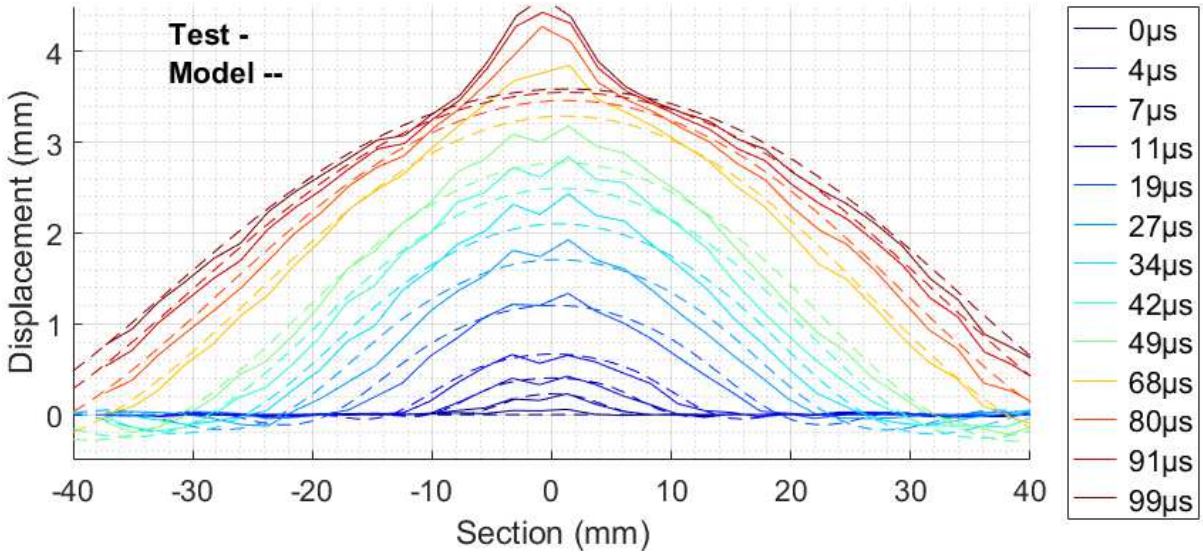

Figure 26 GFRP displacement due to ECF195 explosion confined by 400µm of paint with WFD: Test vs shell

The small bump than can be observed in the central area of the test panel deflection is likely related to the ejection of the paint used for the DIC pattern. This disturbs the profile reconstruction but should not be interpreted as a real local displacement. The deflection profiles between the test and the model are fairly similar. The maximum and the width of displacement are very close. The only main differences concern the maximum strain, as defined in Figure 22, and the waves on each side of the main deflection which are more pronounced in the model than in the test. But this is likely to have second order effect on the damage generation.

The maximum amplitudes of the explosion generated by each ECF wire are of key importance in determining the overpressure profile but this is also the case for the decay profile. The sensitivity analyses presented above are extracted from a modelling considering several decay laws. In order to build a more predictive approach without a supposed decay law, it will be necessary to simulate the confining effect of the paint and the mechanical constraints necessary to eject the paint. For this purpose, mechanical characterization tests of the paint and of the paint adhesive resistance are necessary.

4.2. Effect on a CFRP laminate

The interest of the work done previously was to study the deflection of a panel that has no interaction with the lightning arc. A GFRP panel is highly resistive, therefore all the current from the lightning arc will flow in the LSP, leading to its explosion. The comparison between the simulated deflection from our VDLOAD model and the test results presented fairly good agreement. The next step is now to analyse the effect of this overpressure profile on a CFRP structure for which the interaction with the arc is more complex, especially with the presence of paint that will constrain the arc and lead to current injection into the first plies of the CFRP. The current flow in the CFRP which can generate internal damage due to electro-thermal effects was not considered. As explained in 1.2, the contribution of these effects are supposed negligible in the overall overpressure that will lead to mechanical damage in the composite. Considering now the painted configuration, we can observe on Figure 27 that the deflection profiles are fairly similar between the test of a painted laminate and the simulation of an elastic laminate in the early stages, but not after 60µs. With this simulation with a simple elastic law, since no damage is allowed, the stiffness of the panel is kept constant. But we know that damage and delamination occur early during the lightning test. This delamination could explain the higher deflection profile for the test that is related to the internal damage that reduces the global flexural rigidity of the panel which would increase the deflection of the panel. This is a hypothesis but other contributors could possibly modify the surface load as the arc root constriction which could locally increase the constraint. This would require further investigations.

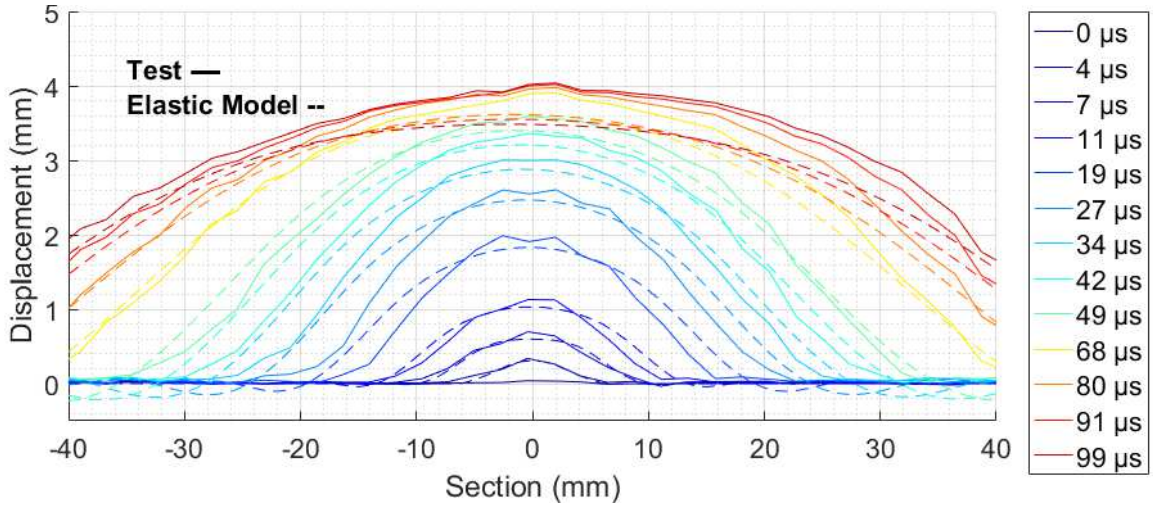

Figure 27 CFRP displacement due to ECF195 explosion confined by 400µm of paint with WFD: Test vs shell

The hypothesis considering that the internal damage of CFRP due to the current flow into the structure can be neglected in the assessment of the total mechanical constraints due to lightning strike tends to be validated by this work. Still, the deflection produced by the load profile validated previously presents some differences with the test which will required additional investigation in the current distribution between the CFRP and the LSP.

4.3. Effect of explosion confinement

As explained previously, the paint thickness has an influence on the confinement of the LSP explosion. In the previous work, we defined a confinement law for the pressure considering 400µm of paint defined in Equation 12 and 13. In order to define the parameters of this law, a sensitivity analysis was necessary, requiring the performance of many model computations. However, this confinement law will be different with another paint thickness. In our lightning test campaign, we assessed the damage and deflection of a CFRP panel protected by ECF195 with different paint thicknesses: 250, 400 and 1000µm. In a first simple approach, we consider the effect of the paint on the confinement based on a linear relationship between the initial decay time and the paint thickness:

$$\begin{cases} \frac{\Delta t_{0_{\delta \mu m}}}{\Delta t_{0_{\beta \mu m}}} = \frac{\delta \mu m}{\beta \mu m} \end{cases} \quad 14$$

The power decay law α was kept identical at 0.8 for all the paint configurations. In addition to adapting the pressure decay law for the pressure amplitude, we used the vaporisation profile measured for the spatio-temporal distribution [13]. The distribution obtained with 200µm of paint, which is close to a diamond shape, was used for the CFRP configuration with 250µm of paint. The distribution with a paint thickness of 550µm is close to an axisymmetric evolution which means that a higher paint thickness will not change the vaporisation profile significantly. Therefore, this distribution was used for the CFRP configuration with 1000µm of paint. Again, the model used here does not consider damage as it leads to disturbance in the displacement. As with our reference configuration with 400µm of paint, the displacement profile is well predicted by this confinement law dependent on paint thickness, as shown in Figure 28:

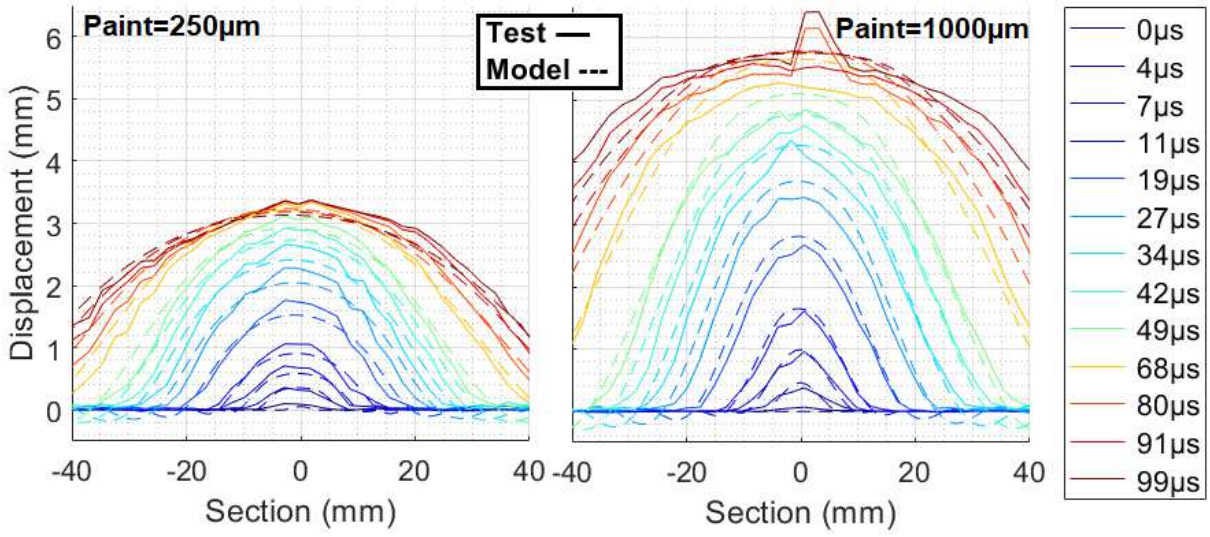

Figure 28 Deflection profile comparison between test and model for different paint thicknesses

The pressure decay due to confinement can be predicted with different paint thicknesses. However, the confinement of the explosion is due, on the one hand, to the paint layer as we demonstrated, but also to the CFRP substrate on the other hand. Considering now a CFRP substrate twice as thick as our baseline, we can assess the influence of the substrate

stiffness in the explosion confinement. If we apply the same mechanical load as our reference configuration (CFRP 13 plies + ECF195 + 400µm of paint) on a configuration that is twice as thick (CFRP 26 plies + ECF195 + 400µm of paint), the deflection profile is higher than expected, as illustrated in Figure 29:

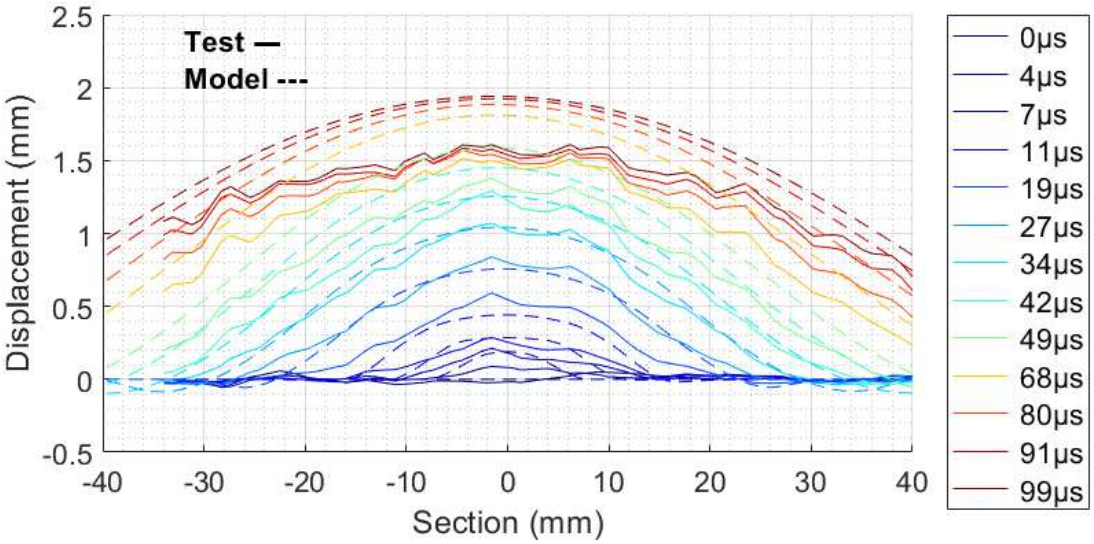

Figure 29 CFRP thick configuration (EDIFISS 100) comparison between test and shell model with reference VDLOAD

A substrate with a higher stiffness sustains the pressure from the explosion more, transferring a higher stress to the paint layer on the top. The paint is ejected more quickly, releasing the pressure of the explosion. This theory is illustrated in Figure 30 below:

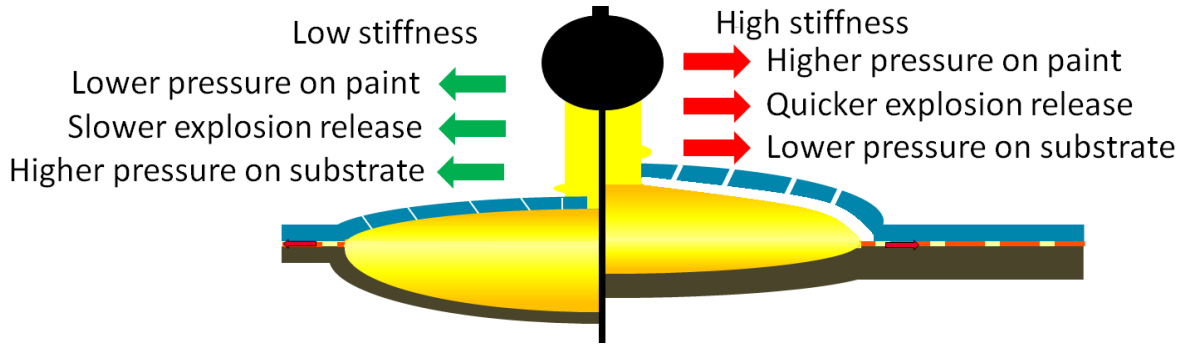

Figure 30 Substrate stiffness influence on explosion release

We can use the laminate theory [30], as explained in 1.2.1, to compare the bending modulus of our reference CFRP panel made of 13 plies and its thicker configuration made of 26 plies.

In this case, the modulus E_f increases from 27GPa to 43GPa. As for the paint thickness impact, we propose to decrease the decay time Δt_0 with the ratio of E_f for the thick configuration. With the introduction of the influence of the panel bending stiffness in the confinement effect, the mechanical load tends to be more representative. As illustrated in Figure 31, the deflection of the panel due to this adapted mechanical load shows better agreement with the test measurement.

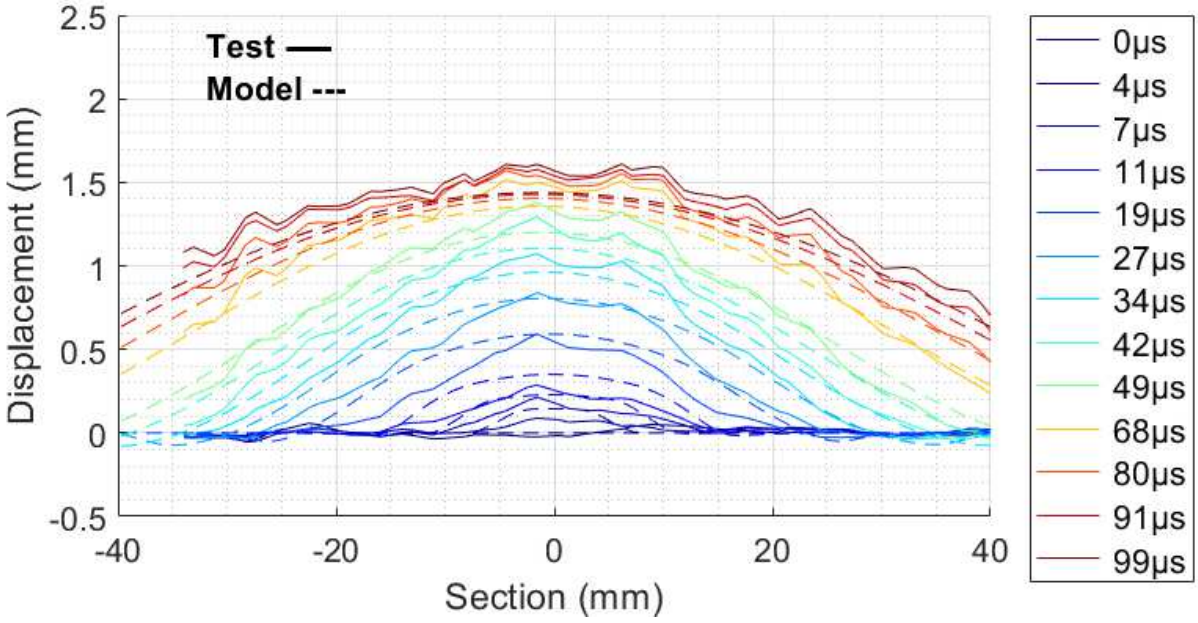

Figure 31 CFRP thick configuration (EDIFISS 100) comparison between test and shell model with adapted VDLOAD

On the same principle, we considered a CFRP structure with a different ply grade i.e., the thickness of the ply is 184µm instead of 127µm for the reference. But the construction comprises 9 plies (90/45/-45/0/90/0/-45/45/90) in order to obtain similar mechanical properties. The equivalent bending modulus is only slightly increased from 27GPa to 28GPa, therefore the same mechanical load as for the reference was applied. As for the reference, the model presents the same deflection in the early stage but the deflection then slows down earlier in comparison to the test results (see Figure 32). The construction of the load dependent on the bending modulus of the panel predicts fairly correctly the displacement of

the panel due to a lightning strike, validating the strong influence of the surface explosion on the mechanical constraints applied on the structure.

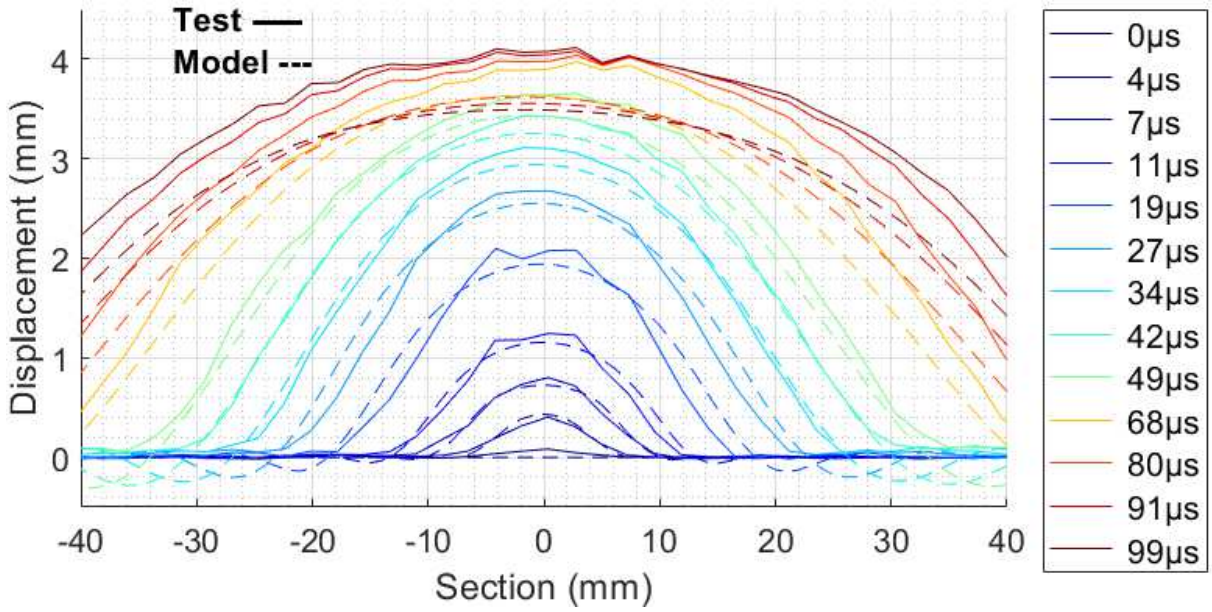

Figure 32 CFRP medium grade comparison between test and shell model with reference VDLOAD

This work on the explosion confinement highlights the importance of considering the lightning load as dependant on the substrate and the paint that will confine the surface explosion and change the amplitude of the overpressure. This is an important conclusion of this work. In order to complete this activity, it will be also necessary to assess its influence on the arc root confinement and therefore on the current distribution and associated explosion profile. As mentioned before, a model simulating the paint layer and its mechanical properties and damage is a necessary step in order to predict the overpressure and avoid the using of a supposed law of pressure distribution and release.

5. Conclusion

The main objective of this paper was to reproduce the mechanical constraints due to a lightning strike. We proposed a methodology to simplify this multiphysics phenomenon into

610 a purely mechanical problem. The ability to reproduce the load produced by the lightning
611 strike is key in order to predict the damage generated by such a phenomenon.
612 From the characterisation of the LSP explosion developed in the previous work which
613 provided the spatio-temporal distribution of the explosion pressure and its amplitude, we
614 could build a complete equivalent mechanical load. In a first step, the explosion pressure
615 was modelled as a pressure applied on the surface of the composite. We built a
616 methodology to convert this profile into a VDLOAD contained in every face of the substrate
617 that will be stressed by the surface explosion pressure. The source of the model input was
618 modified and associated to the user subroutine we developed.
619 In order to validate this model, we chose a set of lightning experimental results which
620 provide essential data. The panel deflection due to the lightning strike was measured thanks
621 to a digital image correlation method.
622 The surface explosion and its confinement by paint were studied independently. Thanks to
623 the use of a GFRP structure which does not divert the lightning current, we were able to
624 study and calibrate the pressure generated by a confined explosion. Since the relaxation
625 time couldn’t be measured independently, a simple law for the pressure decay time was
626 therefore developed, dependent on the maximum explosion pressure. This law simulated
627 the confinement due to the paint which maintains the pressure before being ejected by this
628 underlying explosion pressure. Our study of different paint thicknesses and panel stiffnesses
629 demonstrated the dependency of the pressure profile on the confinement. The LSP
630 explosion is sandwiched by the paint and the composite structure. Therefore, a change in
631 their mechanical properties will influence its confinement and will maintain, or not, a high
632 pressure on the structure. We were able to linearly relate the pressure decay law to the

variation in stiffness of these parts and predict the panel deflection with this simple approach.

The final objective and the next step are to enable the damage prediction with a mechanical model considering the surface load defined in this work.

6. Acknowledgements

This research was supported by EDIFISS project and funded by Airbus. DGA-TA is gratefully thanked for the tests results used in this study. The laboratories ICA and GREMI are gratefully thanked for their help and collaboration. This work was performed using HPC resources from CALMIP (Grant 2019-P19051).

7. References

[1] Plumer, J. A. *Aicraft Lightning Protection Handbook*. Lightning Technologies, Inc., 1989.

[2] Bigand, A., Espinosa, C., Bauchire, J. M., Flourens, F., and Lachaud, F. Lightning Damage Assessment into Composite Based on Surface Explosion and Fiber Breakage. Presented at the International Conference on Composite Materials (ICCM22), Melbourne (Australia), 2019.

[3] Abdelal, G., and Murphy, A. "Nonlinear Numerical Modelling of Lightning Strike Effect on Composite Panels with Temperature Dependent Material Properties." *Composite Structures*, Vol. 109, 2014, pp. 268–278. https://doi.org/10.1016/j.compstruct.2013.11.007.

[4] Fu, K., Ye, L., Chang, L., Yang, C., and Zhang, Z. "Modelling of Lightning Strike Damage to CFRP Composites with an Advanced Protection System. Part I: Thermal-Electrical Transition." *Composite Structures*, Vol. 165, 2017, pp. 83–90. https://doi.org/10.1016/j.compstruct.2017.01.008.

[5] Foster, P., Abdelal, G., and Murphy, A. "Understanding How Arc Attachment Behaviour Influences the Prediction of Composite Specimen Thermal Loading during an Artificial Lightning Strike Test." *Composite Structures*, Vol. 192, 2018, pp. 671–683. https://doi.org/10.1016/j.compstruct.2018.03.039.

[6] Guo, Y., Dong, Q., Chen, J., Yao, X., Yi, X., and Jia, Y. "Comparison between Temperature and Pyrolysis Dependent Models to Evaluate the Lightning Strike Damage of Carbon Fiber Composite Laminates." *Composites Part A: Applied Science and Manufacturing*, Vol. 97, 2017, pp. 10–18. https://doi.org/10.1016/j.compositesa.2017.02.022.

[7] Wang, F. S., Ji, Y. Y., Yu, X. S., Chen, H., and Yue, Z. F. "Ablation Damage Assessment of Aircraft Carbon Fiber/Epoxy Composite and Its Protection Structures Suffered from Lightning Strike." *Composite Structures*, Vol. 145, 2016, pp. 226–241. https://doi.org/10.1016/j.compstruct.2016.03.005.

[8] Ogasawara, T., Hirano, Y., and Yoshimura, A. "Coupled Thermal-Electrical Analysis for Carbon Fiber/Epoxy Composites Exposed to Simulated Lightning Current." *Composites Part A: Applied Science and Manufacturing*, Vol. 41, No. 8, 2010, pp. 973–981. https://doi.org/10.1016/j.compositesa.2010.04.001.

[9] Dong, Q., Guo, Y., Chen, J., Yao, X., Yi, X., Ping, L., and Jia, Y. "Influencing Factor Analysis Based on Electrical-Thermal-Pyrolytic Simulation of Carbon Fiber Composites Lightning Damage."

Composite Structures, Vol. 140, 2016, pp. 1–10. https://doi.org/10.1016/j.compstruct.2015.12.033.

[10] Chippendale, R. *Modelling of the Thermal Chemical Damage Caused to Carbon Fibre Composites*. University of Southampton, 2013.

[11] Sun, J., Li, Y., Tian, X., Duan, Y., Yao, X., and Wang, B. "Experimental and Numerical Analysis of Damage Mechanisms for Carbon Fiber-Reinforced Polymer Composites Subjected to Lightning Strikes." *Engineering Failure Analysis*, Vol. 118, 2020, p. 104894. https://doi.org/10.1016/j.engfailanal.2020.104894.

[12] Sun, J., Tian, X., Li, Y., Wu, Y., Duan, Y., Chen, J., Ziegmann, G., Rong, M., Yao, X., and Wang, B. "Lightning Strike-Induced Dynamic Conduction Characteristics and Damage Behavior of Carbon Fiber-Reinforced Polymer Composites." *Composite Structures*, Vol. 275, 2021, p. 114391. https://doi.org/10.1016/j.compstruct.2021.114391.

[13] Bigand, A., Espinosa, C., and Bauchire, J.-M. Lightning Surface Explosion Impact Study on Damage Generation into Composite. Presented at the ICOLSE 2019, Wichita (USA), 2019.

[14] Lee, J., Lacy Jr., T. E., and Pittman Jr., C. U. "Coupled Thermal Electrical and Mechanical Lightning Damage Predictions to Carbon/Epoxy Composites during Arc Channel Shape Expansion." *Composite Structures*, Vol. 255, 2021, p. 112912. https://doi.org/10.1016/j.compstruct.2020.112912.

[15] Ma, X., Wang, F., Wang, Z., Li, Y., and Xu, B. "Thermal Dynamic Damage of Aircraft Composite Material Suffered from Lightning Channel Attachment Based on Moving Mesh Method." *Composites Science and Technology*, Vol. 214, 2021, p. 109003. https://doi.org/10.1016/j.compscitech.2021.109003.

[16] Karch, C. Contributions of Lightning Current Pulses to Mechanical Damage of CFRP Structures. Presented at the ICOLSE, Toulouse, 2015.

[17] Chemartin, L., Lalande, P., Peyrou, B., Chazottes, A., Elias, P. Q., Delalondre, C., Cheron, B. G., and Lago, F. "Direct Effects of Lightning on Aircraft Structure: Analysis of the Thermal, Electrical and Mechanical Constraints." *AerospaceLab*, No. 5, 2012, p. p-1.

[18] Soulas, F., Espinosa, C., Lachaud, F., Guinard, S., Lepetit, B., Revel, I., and Duval, Y. "A Method to Replace Lightning Strike Tests by Ball Impacts in the Design Process of Lightweight Composite Aircraft Panels." *International Journal of Impact Engineering*, Vol. 111, 2018, pp. 165–176.

[19] Gineste, P.-N., Clerc, R., Castanie, C., Andreu, H., and Buzaud, E. Assessment of Lightning Direct Effects Damages by Modelling Techniques. Presented at the ICOLSE, Pittsfield, USA, 2009.

[20] Kawakami, H. *Lightning Strike Induced Damage Mechanisms of Carbon Fiber Composites*. Ph.D. University of Washington, United States -- Washington, 2011.

[21] Muñoz, R., Delgado, S., González, C., López-Romano, B., Wang, D.-Y., and LLorca, J. "Modeling Lightning Impact Thermo-Mechanical Damage on Composite Materials." *Applied Composite Materials*, Vol. 21, No. 1, 2014, pp. 149–164. https://doi.org/10.1007/s10443-013-9377-9.

[22] Lee, J., Lacy, T. E., and Pittman, C. U. "Lightning Mechanical Damage Prediction in Carbon/Epoxy Laminates Using Equivalent Air Blast Overpressure." *Composites Part B: Engineering*, Vol. 212, 2021, p. 108649. https://doi.org/10.1016/j.compositesb.2021.108649.

[23] Lee, J., Lacy, T. E., Pittman, C. U., and Reddy, J. N. "Numerical Estimations of Lightning-Induced Mechanical Damage in Carbon/Epoxy Composites Using Shock Wave Overpressure and Equivalent Air Blast Overpressure." *Composite Structures*, Vol. 224, 2019, p. 111039. https://doi.org/10.1016/j.compstruct.2019.111039.

[24] Lepetit, B., Escure, C., Guinard, S., Revel, I., and Peres, G. Thermo-Mechanical Effects Induced by Lightning on Carbon Fiber Composite Materials. Presented at the ICOLSE, Oxford, UK, 2011.

[25] Soulas, F. *Développement d'un Modèle Mécanique Pour La Prédiction Des Dommages de Panneaux Composites Aéronautiques Soumis à Un Choc Foudre*. Toulouse, ISAE, 2016.

[26] Kumar, V., Yokozeki, T., Karch, C., Hassen, A. A., Hershey, C. J., Kim, S., Lindahl, J. M., Barnes, A., Bandari, Y. K., and Kunc, V. "Factors Affecting Direct Lightning Strike Damage to Fiber

Reinforced Composites: A Review." *Composites Part B: Engineering*, Vol. 183, 2020, p. 107688. https://doi.org/10.1016/j.compositesb.2019.107688.
[27] EUROCAE. *ED-84: Aircraft Lightning Environment And Related Test Waveforms*. 1997.
[28] Lago, F., Fontaine, G., and Larrieu, C. Measurement by a Digital Image Correlation Technique of the Deflection of Panels Submitted to Lightning Impulse. Presented at the ICOLSE, Oxford, UK, 2011.
[29] Jia, S., Wang, F., Xu, B., and Yan, W. "A Developed Energy-Dependent Model for Studying Thermal Shock Damage and Phase Transition of Composite Reinforced Panel Subjected to Lightning Strike." *European Journal of Mechanics - A/Solids*, Vol. 85, 2021, p. 104141. https://doi.org/10.1016/j.euromechsol.2020.104141.
[30] Gay, D. *Matériaux Composites*. 1997.
[31] Bigand, A. *Damage Assessment on Aircraft Composite Structure Due to Lightning Constraints*. Institut Supérieur de l'Aéronautique et de l'Espace, Toulouse, 2020.
[32] Naghipour, P., Pineda, E. J., and Arnold, S. M. "Simulation of Lightning-Induced Delamination in Un-Protected CFRP Laminates." *Applied Composite Materials*, Vol. 23, No. 4, 2016, pp. 523–535. https://doi.org/10.1007/s10443-016-9472-9.
[33] Karch, C., Schreiner, M., Honke, R., and Wolfrum, J. Shock Waves from a Lightning Discharge. Presented at the 2018 34th International Conference on Lightning Protection (ICLP), 2018.